A Study of Alkaline-Based H_2-Br_2 and H_2-I_2 Reversible Fuel Cells

Regis P. Dowd Jr.,[a,*] Venkata Yarlagadda,[a] Dhrubajit Konwar,[a] Guangyu Lin,[b,] Guoming Weng,[c] Chi-Ying Vanessa Li,[c] Kwong-Yu Chan,[c,**] and Trung Van Nguyen[a,***,z]**

[a]*Department of Chemical & Petroleum Engineering, The University of Kansas, Lawrence, Kansas 66045, USA*
[b]*TVN Systems, Inc., Lawrence, Kansas 66046, USA*
[c]*Department of Chemistry, The University of Hong Kong, Hong Kong SAR, People's Republic of China*

The hydrogen-bromine (H_2-Br_2) and hydrogen-iodine (H_2-I_2) reversible fuel cell systems can be operated in the acid or alkaline modes. The alkaline versions were evaluated because of the advantages over the acidic systems such as higher cell potential, lower corrosivity, and lower catalyst cost for the hydrogen evolution and oxidation reactions. Fuel cells were assembled to validate the operational feasibility of the alkaline systems and to evaluate their performance. The results confirmed that the alkaline H_2-Br_2 and H_2-I_2 fuel cells have a higher cell voltage than their corresponding acidic systems while maintaining similarly fast electrode reaction kinetics. However, the performance of these alkaline fuel cells is currently limited by the low ionic conductivity of the K^+ form membranes, which is attributed to the slow diffusivity of the larger K^+ ion in these membranes, and providing equal access of gaseous and liquid reactants to the active sites for the hydrogen reaction. These limitations could be overcome by using thinner membranes, operating the fuel cell at higher concentrations and temperatures, and development of porous electrodes with better two-phase fluid distribution.

© The Author(s) 2016. Published by ECS. This is an open access article distributed under the terms of the Creative Commons Attribution Non-Commercial No Derivatives 4.0 License (CC BY-NC-ND, http://creativecommons.org/licenses/by-nc-nd/4.0/), which permits non-commercial reuse, distribution, and reproduction in any medium, provided the original work is not changed in any way and is properly cited. For permission for commercial reuse, please email: oa@electrochem.org. [DOI: 10.1149/2.0011614jes] All rights reserved.

BY-NC-ND

Manuscript submitted August 8, 2016; revised manuscript received September 21, 2016. Published October 20, 2016. This was Paper 615 presented at the Cancun, Mexico, Meeting of the Society, October 5–9, 2014.

The acidic hydrogen-bromine (H_2-Br_2) reversible fuel cell has been an attractive system for electrical energy storage because of its high round-trip conversion efficiency, high power density capability, and anticipated low costs. Since HBr solution serves as both the electrolyte and active materials for the fuel cell, no supporting electrolyte is needed. This aspect results in higher energy density; therefore, sparking great interest in this system for energy storage.[1–12] While all previous studies have been with the acidic system, the H_2-Br_2 fuel cell system can also be operated in the alkaline mode. However, this mode had not been studied until recently.[13]

In an acidic H_2-Br_2 fuel cell, the charge and discharge electrode reactions are as follows:

$$Br_2(+)Electrode:\ 2HBr \underset{discharge}{\overset{charge}{\rightleftarrows}} Br_2+2H^++2e^-,\ \boldsymbol{E^o_{red} = +1.09\,V} \quad [1]$$

$$H_2(-)Electrode:\quad 2H^+ + 2e^- \underset{discharge}{\overset{charge}{\rightleftarrows}} H_2,\ \boldsymbol{E^o_{red} = +0.0\,V} \quad [2]$$

All reported voltages are relative to the standard hydrogen electrode (SHE). During charge, the H^+ ions migrate from the Br_2 side across a proton conducting membrane (e.g., Nafion) to the H_2 side to maintain electroneutrality and charge balance. The process described above is reversed during discharge. The overall reaction is given below, with the standard cell potential of +1.09 V.

$$Overall\,Reaction:\ 2HBr \underset{discharge}{\overset{charge}{\rightleftarrows}} Br_2+H_2,\ \boldsymbol{E^o_{cell} = +1.09\,V} \quad [3]$$

In an alkaline H_2-Br_2 fuel cell, the charge and discharge electrode reactions are as follows:

$$Br_2(+)Electrode:\ 2KBr \underset{discharge}{\overset{charge}{\rightleftarrows}} Br_2+2K^++2e^-,\ \boldsymbol{E^o_{red}=+1.09\,V} \quad [4]$$

$$H_2(-)Electrode:\quad 2H_2O + 2e^- \underset{discharge}{\overset{charge}{\rightleftarrows}} H_2 + 2OH^-,\ \boldsymbol{E^o_{red} = -0.83\,V} \quad [5]$$

During charge, the cations (e.g., K^+ when KOH and KBr are used) associated with the Br^- ions at the positive Br_2 electrode migrate across a cation (K^+) conducting membrane to the negative H_2 side, and vice versa during discharge, and combine with the OH^- ions to form KOH as shown in the overall reaction below. The processes described above are reversed during discharge. With these electrode reactions, the standard cell potential is +1.92 V.

$$Overall\,Reaction:\quad 2KBr + 2H_2O \underset{discharge}{\overset{charge}{\rightleftarrows}} H_2 + Br_2 + 2KOH,\ \boldsymbol{E^o_{cell} = +1.92\,V} \quad [6]$$

Note that in an acidic H_2-Br_2 system, the H^+ ion is the ionic carrier and in an alkaline H_2-Br_2 system, the K^+ ion (when KOH and KBr are used) is the ionic carrier. Based on the reactions shown above, the alkaline system offers a higher cell voltage, which is an advantage because of its potentially higher power output and higher energy density. The other advantages of this system include the fact that non-noble catalysts can be used for the hydrogen reactions and lower corrosiveness of KBr and KOH solutions relative to the HBr solution used in the acidic system.[14,15] The primary challenge is anticipated to be the three-phase hydrogen electrode reaction involving a solid electronic conducting phase and a two-phase reactant system consisting of gaseous hydrogen and aqueous KOH.

Similar to the H_2-Br_2 system, the hydrogen-iodine (H_2-I_2) system can also be operated in the acidic and alkaline modes. The acidic version of the H_2-I_2 fuel cell was evaluated but not pursued by our group because of its low overall standard cell potential. While the iodine reactions have been found in many applications including dye sensitized solar cells,[16,17] very few studies have been reported that use the iodine reaction in a flow battery or reversible fuel cell application.[18–20] Taking advantage of the higher overall reaction potential in alkaline solutions, we decided to evaluate the alkaline hydrogen-iodine fuel cell system because of the lower toxicity of iodine as compared to bromine.

*Electrochemical Society Student Member.
**Electrochemical Society Member.
***Electrochemical Society Fellow.
[z]E-mail: cptvn@ku.edu

Downloaded on 2017-07-31 to IP 147.8.230.58 address. Redistribution subject to ECS terms of use (see ecsdl.org/site/terms_use) unless CC License in place (see abstract).

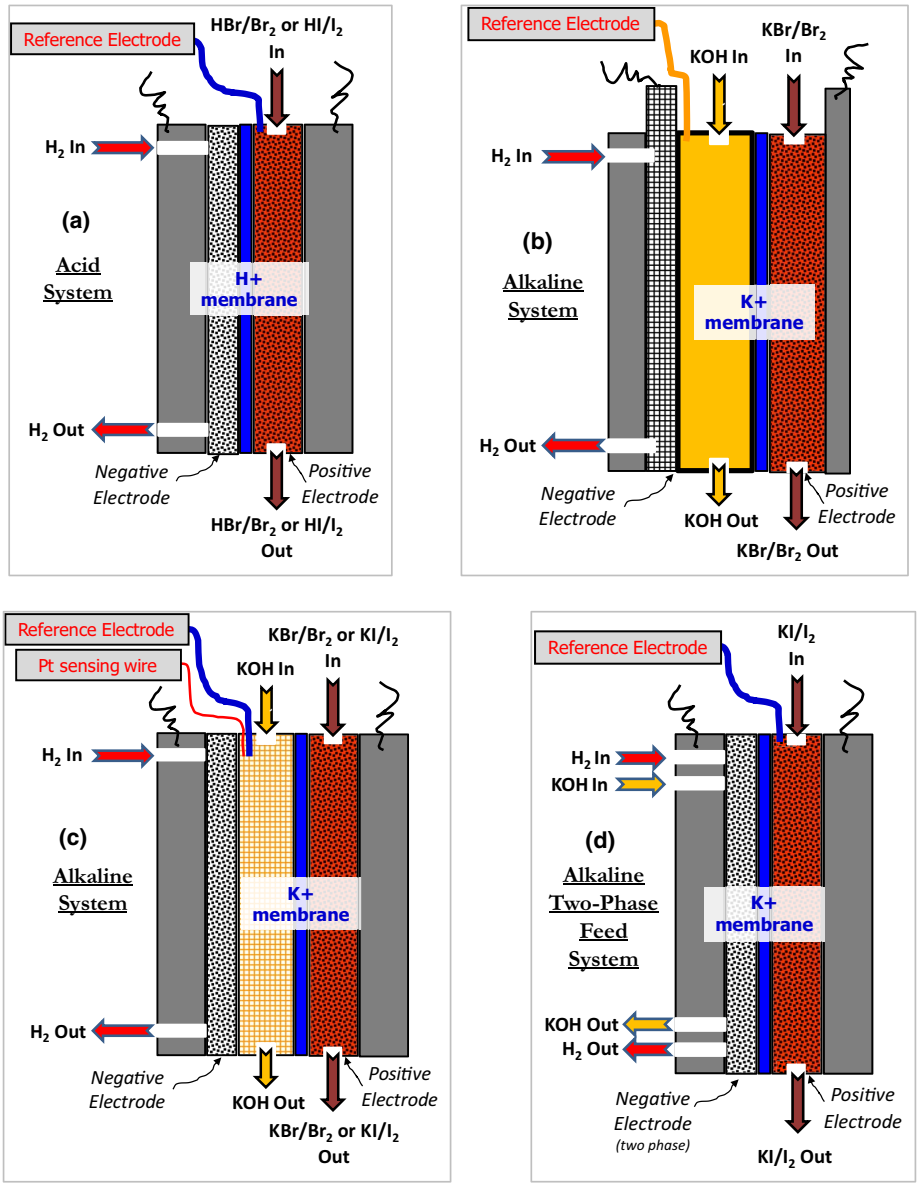

Figure 1. Cell configurations for the (a) acid-based H_2-Br_2 and H_2-I_2 reversible fuel cell systems, (b) alkaline-based H_2-Br_2 reversible fuel cell (Study 1), (c) single-phase feed for the alkaline-based H_2-Br_2 and H_2-I_2 reversible fuel cells (Study 2 and Study 3), and (d) two-phase feed for the alkaline-based H_2-I_2 reversible fuel cell (Study 4).

Acidic Mode:

$$I_2(+)Electrode\text{: } 2HI \underset{discharge}{\overset{charge}{\rightleftarrows}} I_2+2H^+ +2e^-,\ E^o{}_{red}=+0.54\,V \quad [7]$$

$$H_2(-)Electrode\text{: } 2H^+ + 2e^- \underset{discharge}{\overset{charge}{\rightleftarrows}} H_2,\ E^o{}_{red} = +0.0\,V \quad [8]$$

$$Overall Reaction\text{: } 2HI \underset{discharge}{\overset{charge}{\rightleftarrows}} I_2+H_2,\ E^o{}_{cell} = +0.54\,V \quad [9]$$

Alkaline Mode (with KOH/KI solutions)

$$I_2(+)Electrode\text{: } 2KI \underset{discharge}{\overset{charge}{\rightleftarrows}} I_2 + 2K^+ + 2e^-,\quad E^o{}_{red} = +0.54\,V \quad [10]$$

$$H_2(-)Electrode\text{: } 2H_2O + 2e^- \underset{discharge}{\overset{charge}{\rightleftarrows}} H_2 + 2OH^-,\quad E^o{}_{red} = -0.83\,V \quad [11]$$

$$Overall Reaction\text{: } 2KI + 2H_2O \underset{discharge}{\overset{charge}{\rightleftarrows}} H_2 + I_2 + 2KOH,\quad E^o{}_{cell} = +1.37\,V \quad [12]$$

In this paper, alkaline H_2-Br_2/H_2-I_2 fuel cells were assembled in multiple configurations, as shown in Figure 1, and tested to validate the concept and feasibility of the alkaline H_2-Br_2 and H_2-I_2 fuel cell systems. A schematic of the acid-based H_2-Br_2/H_2-I_2 fuel cell (Figure 1a) tested in our previous studies[2,6,10–12] was also included to illustrate the difference between the acid-based and alkaline-based (Figures 1b and 1c) cell configurations, mainly the use of an additional electrolyte compartment for the KOH solution at the hydrogen electrode. Figure 1d shows the configuration used to evaluate the performance of the alkaline H_2-I_2 fuel cell with two-phase reactant feed to the hydrogen electrode. In this two-phase feed configuration, the KOH electrolyte compartment was eliminated and a single two-phase feed consisting

Downloaded on 2017-07-31 to IP 147.8.230.58 address. Redistribution subject to ECS terms of use (see ecsdl.org/site/terms_use) unless CC License in place (see abstract).

Table I. Experimental Conditions.

Study #	1	2	3	4
System	Alkaline H_2-Br_2	Alkaline H_2-Br_2	Alkaline H_2-I_2	Alkaline H_2-I_2
Cell Configuration	Figure 1b	Figure 1c	Figure 1c	Figure 1d
Negative Electrode	Nickel screen coated with Pt/C/PTFE (1.2 mg Pt/cm^2)	SGL 35BC GDL coated with Pt/C/PTFE layer (0.8 mg Pt/cm^2)	SGL 35BC GDL coated with Pt/C/PTFE layer (0.8 mg Pt/cm^2)	10% wet-proof Toray 060 GDL coated with Pt/C/PTFE layer (0.8 mg Pt/cm^2)
Positive Electrode	Solid carbon plate	2 layers of SGL 10AA	2 layers of SGL 10AA	Carbon nanotube GDL
Membrane	K^+-form of Nafion 117	K^+-form of Nafion 212 and K^+-form of Nafion 115	K^+-form of Nafion 212	K^+-form of Nafion 212
Flow Fields	H_2 electrode - carbon interdigitated flow field; Br_2 electrode - carbon interdigitated flow field	H_2 electrode - carbon interdigitated flow field; Br_2 electrode - tantalum interdigitated flow field	H_2 electrode - carbon interdigitated flow field; Br_2 electrode - tantalum interdigitated flow field	H_2 electrode - carbon interdigitated flow field; Br_2 electrode - carbon interdigitated flow field
Electrolyte Compositions	1 M KBr/0.5 M Br_2 solution for the bromine electrode, 1 M KOH solution and H_2 gas for the hydrogen electrode	1 M KBr/0.3 M Br_2 solution for the bromine electrode, 1 M/3 M KOH solution and H_2 gas for the hydrogen electrode	1 M KBr/0.4 M I_2 solution for the iodine electrode, 1 M/2 M/3 M KOH solution and H_2 gas for the hydrogen electrode	1 M KBr/0.4 M I_2 solution for the iodine electrode, 3 M KOH solution and H_2 gas for the hydrogen electrode
Additional Details	KOH Reservoir used in conjunction with a PTFE gas distributor plate at the H_2 electrode	1 mm glass-fiber mat served as an electrolyte reservoir for the KOH solution	1 mm glass-fiber mat served as an electrolyte reservoir for the KOH solution	2 phase reactant feed flow for H_2/KOH

of gaseous hydrogen and aqueous KOH solution was simultaneously injected into the hydrogen electrode. This configuration looks very similar to the simpler acidic H_2-I_2 fuel cell configuration with the exception of the two-phase feed and K^+ membrane. The elimination of the KOH solution compartment and the use of two-phase feed injection were expected to greatly reduce the cell internal ohmic resistance and simplify the cell design.

As shown in Figure 1, a saturated calomel reference electrode (SCE) was used to separate the cell voltages into half-cell voltages. The half-cell voltages were used to validate that the high cell voltages obtained were from the more negative potential of the hydrogen reaction in an alkaline solution and to help identify the cell components impacting fuel cell performance the most. The reference electrode was connected to either the KOH electrolyte compartment using a KOH electrolyte bridge made of the same KOH solution or the iodine compartment using a KI salt bridge. For the cell configuration shown in Figure 1c, a platinum wire was also inserted into the KOH compartment to separate the full cell impedance into half-cell impedances during electrochemical impedance spectroscopy (EIS) measurements.

Experimental

The K^+ conducting membranes used for the alkaline H_2-Br_2 fuel cells were prepared by boiling H^+ conducting Nafion membranes in KOH solutions (1 M–5 M) for 1–4 hr to convert them to K^+ form. After the membranes were boiled in KOH solutions, they were cooled to room temperature, rinsed with de-ionized water and used with no further treatment. A significant increase in the K^+ conductivity was observed between membranes treated in 1 M and 3 M KOH solutions. However, no significant changes in the K^+ conductivity were observed between membranes treated in 3 M and 5 M KOH solutions. The results supported the hypothesis that since the ion (H^+ or SO_3^-) concentration in Nafion 1100 equivalent weight membranes is about 1.8 M, the membranes need to be boiled in KOH solutions with molarities equal to or higher than 1.8 M in order to replace the H^+ ions in these membranes with K^+ ions. Higher K^+ concentration provides a higher driving force to overcome the higher affinity of the SO^{3-} groups for the H^+ ions. Nafion membranes treated in 3 M KOH solution were used for all studies presented in this work.

Four different fuel cell studies were conducted, all at room temperature (~22°C). Table I summarizes the experimental conditions for each study. In the first study, discharge and charge performances were collected to validate the concept and feasibility of the alkaline H_2-Br_2 system. The cell configuration for the first study is shown in Figure 1b. A nickel screen coated with a layer of Pt/C/PTFE containing 1.2 mg Pt/cm^2 geometric area was used as the hydrogen electrode and a solid carbon plate was used as the bromine electrode, both with active geometric area of approximately 4 cm^2. The PTFE phase was added to the hydrogen electrode to create a hydrophobic porous structure for hydrogen gas transport. Even though our ultimate goal is to test this system with a non-noble catalyst (e.g., nickel or nickel alloys[14,15]) for the hydrogen reaction, platinum on carbon support was used as the catalyst in the hydrogen electrodes for these studies. Electrical current was collected from the edges of the electrodes. A potassium ion (K^+) conducting Nafion 117 (~178 μm thick) membrane was used to facilitate potassium ion transport between the two electrodes and to keep the hydroxide, bromine and bromide anions from crossing from one side to the other. 1 M KBr/0.5 M Br_2 solution was recirculated through the bromine electrode and 1 M KOH solution was recirculated through the hydrogen electrode. Positive and negative electrolyte volumes were 500 mL and 300 mL, respectively, for all studies. The KOH solution was fed to the KOH reservoir on one side of the hydrogen electrode while hydrogen gas at ambient pressure was fed to the opposite side from a PTFE gas distributor plate, both at 10 mL/min, as shown in Figure 1b. A SCE was inserted into the KOH chamber and used as a reference electrode. The reference electrode enables us to separate the overall cell voltage into individual electrode voltages during open circuit, as well as during discharge and charge. The discharge and charge polarization curves were obtained by applying constant potential in staircase mode from open circuit voltage (OCV) to +/− 300 mV in increments of 50 mV. The cell was held at each potential for at least 2 minutes in order for the cell to reach steady state. All electrode voltages reported in this paper have been converted to SHE basis.

In the second study, the cell was modified to improve the performance of the alkaline H_2-Br_2 system. The cell configuration for the second study is shown in Figure 1c. The hydrogen electrode was made by applying a Pt/C/PTFE layer onto the micro-porous layer (MPL) side of a bilayer Sigracet GDL-35BC carbon gas diffusion medium. The catalyst loading was approximately 0.8 mg Pt/cm^2 geometric area, and the electrode geometric active surface area was about 2.25 cm^2 (1.5 cm × 1.5 cm). Two layers of Sigracet carbon gas diffusion layers (10AA) were used as the bromine electrode. Potassium ion (K^+)-form Nafion 212 (~51 μm thick) and 115 (~127 μm thick) membranes treated in 3 M KOH were used in this study to evaluate the effect of membrane thickness on fuel cell performance. A layer of glass-fiber mat (purchased from 3 M) with a thickness of approximately 1 mm was placed between the hydrogen electrode and the

Downloaded on 2017-07-31 to IP 147.8.230.58 address. Redistribution subject to ECS terms of use (see ecsdl.org/site/terms_use) unless CC License in place (see abstract).

membrane to serve as an electrolyte reservoir for the KOH solution and to allow the cell components to be compressed to establish good electrical contact between the electrodes and the flow field/current collector plates. In order to study the effect of KOH concentration, KOH solutions at 1 M and 3 M were fed to the KOH reservoir side of the hydrogen electrode at flow rates between 0.6 and 0.95 mL/min with a peristaltic pump (Masterflex EW-77122-14) while neat hydrogen gas at about 121 kPa absolute was fed to the other side of the electrode at a rate of approximately 660 mL/min using a recirculation pump. At the bromine electrode, a solution of 1 M KBr/0.3 M Br_2 was fed at a flow rate of 1.5 mL/min with a peristaltic pump (Stenner EW-74206). This Br_2 flow rate is equivalent to 1.45 A/cm^2 or more than 12 times the maximum current densities obtained in this study. The high flow rate and excess electrolyte used in this study represent attempts to ensure that the bromine concentration over the entire electrode's outer surface was constant during the discharge and charge cycle. A carbon interdigitated flow field[21,22] was used at the hydrogen electrode and a tantalum interdigitated flow field was used at the bromine electrode to reduce the mass transport resistance in the electrodes. Electrical current collection at the negative electrode was from the edge of a stainless steel plate placed in contact with the carbon flow field block. Electrical current collection at the positive electrode was directly from the edge of the tantalum flow field plate. Similar to the first study, the discharge and charge curves were measured using constant potential in staircase mode from OCV to +/− 500 mV in increments of 50 mV and a step duration of 5 minutes (or long enough to obtain a steady state current). EIS (Gamry EIS 300) was conducted at 5 mV amplitude over a frequency range of 1 Hz to 100 kHz to measure the internal resistance of the entire fuel cell operated with different KOH solutions and membrane thicknesses.

In the third and fourth studies, two cell configurations were tested to evaluate the performance of an alkaline H_2-I_2 fuel cell. The first cell configuration, shown in Figure 1c, consisted of a single-phase reactant feed for the negative electrode. The second cell configuration, shown in Figure 1d, consisted of a two-phase reactant feed for the negative electrode. For the single-phase feed case (Study 3), we used the same cell components as the alkaline H_2-Br_2 fuel cell in the second study. To study the effect of KOH concentration on fuel cell performance, KOH solutions at 1 M, 2 M and 3 M were fed to the KOH reservoir side of the hydrogen electrode at flow rates between 0.6 and 0.95 mL/min with a peristaltic pump while neat hydrogen gas at about 134 kPa absolute was fed to the other side of the electrode at a rate of approximately 660 mL/min using a recirculation pump. At the iodine electrode, a solution of 1 M KBr/0.4 M I_2 was fed at a flow rate of 1.5 mL/min with a peristaltic pump, corresponding to about 1.93 A/cm^2. This high flow rate and excess electrolyte represent attempts to ensure that the iodine concentration over the entire electrode's outer surface was constant during the discharge and charge cycle. Nafion 212 membrane in K^+-form was used in all H_2-I_2 runs.

For the two-phase feed case (Study 4), the KOH compartment was removed and different negative and positive electrode materials were used. 3 M KOH solution was recirculated through the negative electrode and the KOH flow rate was adjusted to obtain good performance. The best KOH flow rates were found to be 5.1 ml/min during discharge and 11.5 ml/min during charge. Higher KOH flow rate during charge was needed to purge the hydrogen gas generated in the negative electrode. An interdigitated flow field ensured that liquid KOH solution did not flood the negative porous electrode. To allow both gaseous hydrogen and aqueous KOH to reach the catalyst at the negative electrode, a single-layer 10% wet-proof Toray 060 gas diffusion layer was used as the catalyst layer support. In a previous study, we discovered that a highly hydrophobic MPL prevents liquid from passing through the MPL to reach the catalyst layer. The platinum catalyst loading in the negative electrode was 0.8 mg/cm^2 geometric area. To reduce transport and ohmic resistance while maintaining high active area in the positive electrode, a single layer of carbon nanotube (CNT) gas diffusion layer was used as the positive electrode. The CNT gas diffusion layer was synthesized in our lab for a prior acid-based H_2-Br_2 fuel cell study.[10,11] The same H_2 and KI/I_2 flow rates used in the single-phase feed study were also used here. The main difference for this study is that both H_2 and KOH were injected directly to one side of the negative electrode, versus being injected into the negative electrode from two sides from two separate compartments.

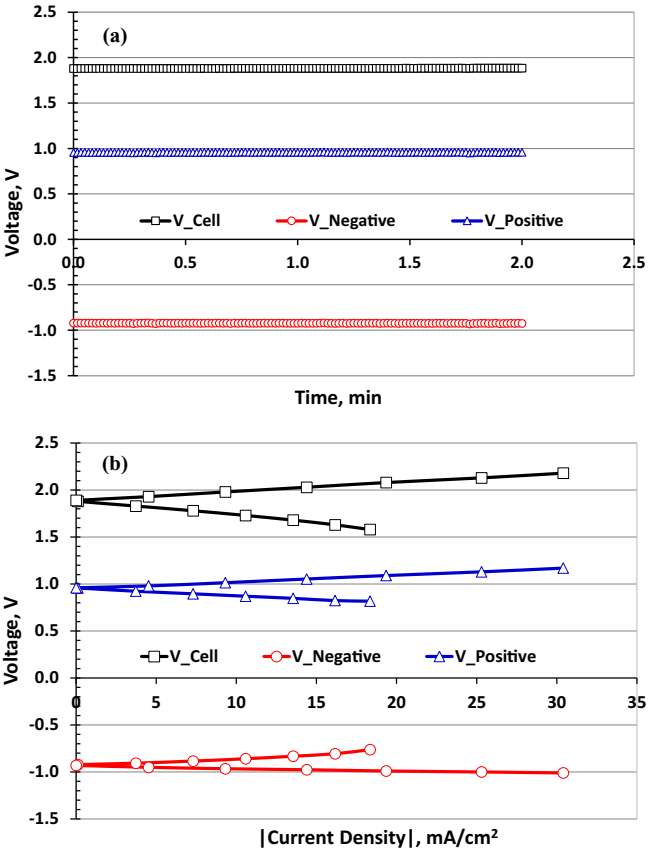

Figure 2. Study 1: Cell and individual electrode potentials of the alkaline H_2-Br_2 fuel cell during (a) open circuit and (b) charge and discharge.

Results and Discussion

Study 1.—The objective of the first study was to validate the concept and feasibility of the alkaline H_2-Br_2 fuel cell system by showing that a higher cell and more negative hydrogen electrode potentials could be obtained, as well as demonstrate reversible discharge and charge performance. Figure 2a shows the cell and the individual half-cell voltages during one of the open circuit steps. Note the higher cell voltage and more negative voltage of the hydrogen electrode as a result of operating the hydrogen reactions in an alkaline (i.e., high pH) solution. Figure 2b shows the charge and discharge performance of the alkaline H_2-Br_2 fuel cell for the first study. The linear discharge and charge curves in Figure 2b suggests that most of the voltage loss in the system is due to ohmic resistances in the cell and confirms that the hydrogen (on platinum) and bromine reactions (on carbon) in the alkaline system are still quite fast. Next, the fact that the discharge curve for the full cell and hydrogen electrode show some mass transport effect at current densities greater than 15 mA/cm^2 highlights that the mass transport effect was at the hydrogen electrode. This mass transport effect could be attributed to the limited hydrogen diffusion rate through the liquid KOH electrolyte layer formed on the hydrophilic active area of the platinum electrode. Finally, the low performance observed in the first study can be attributed to the high internal resistance of the cell (~2.2 ohms). The high internal cell resistance can be attributed to using a thick membrane (183-micron Nafion 117), large gaps for KOH and KBr/Br_2 solutions, and edge current collection, especially for the less conductive solid carbon electrode.

Downloaded on 2017-07-31 to IP 147.8.230.58 address. Redistribution subject to ECS terms of use (see ecsdl.org/site/terms_use) unless CC License in place (see abstract).

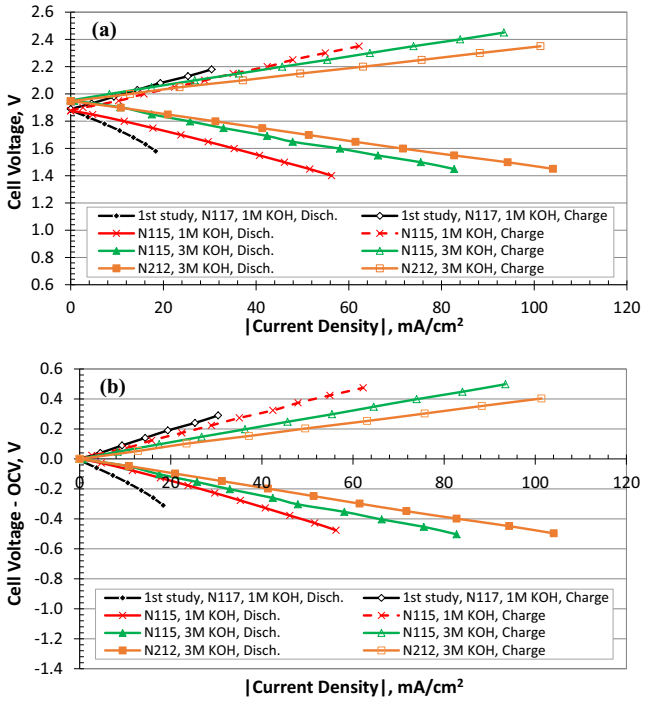

Figure 3. Studies 1 and 2: Effect of membrane thickness and KOH concentration on the performance of the alkaline H_2-Br_2 fuel cells, cell overpotential (cell voltage-OCV) was used in (b) to correct for different OCVs.

Study 2.—After the concept and feasibility of the alkaline H_2-Br_2 fuel cell were validated in study 1, a second study was conducted to see if higher performance could be obtained by making some modifications to the cell design. Modifications included using a porous hydrogen electrode with higher platinum catalyst surface area, thinner membranes, higher KOH concentration, and a porous bromine electrode with higher active surface area. For the hydrogen electrode, a high surface area porous electrode, similar to those used in H_2-O_2 proton exchange membrane fuel cells, was used. For the bromine electrode, two layers of porous carbon diffusion media instead of a solid carbon electrode were used to increase the active surface area. By using a porous electrode in which the positive electrolyte could be introduced into the electrode from the surface next to the flow field, the positive electrolyte compartment between the positive electrode and the membrane was eliminated. Carbon (for H_2) and tantalum (for Br_2) interdigitated flow field plates were used. Electrical current was collected in the direction normal to the surface of the electrodes as in a regular fuel cell. In this configuration, a porous glass-mat KOH reservoir layer was needed between the hydrogen electrode and the membrane to allow the cell to be compressed so that good electrical contact could be obtained between the electrodes and the current collector flow plates. Finally, thinner and less resistive membranes, 51-micron thick Nafion 212 and 127-micron thick Nafion 115, and higher (3 M) KOH concentration were used to evaluate their effects on the fuel cell internal resistance and performance.

For study 2, Figure 3a shows the discharge and charge performance of the improved alkaline H_2-Br_2 fuel cell. The performance of the fuel cell in the first study was also included for comparison. Higher KOH concentration leads to more negative hydrogen electrode potential as described by the Nernst equation, thus higher cell OCV. To better illustrate the changes in the slope of the curves on the graph, the results in Figure 3a are replotted in Figure 3b where the vertical axis is changed to the cell voltage minus the OCV (i.e., essentially the overpotential of the fuel cell). In this format, we can clearly see the effect of membrane thickness and KOH concentration on the slope of the polarization curves.

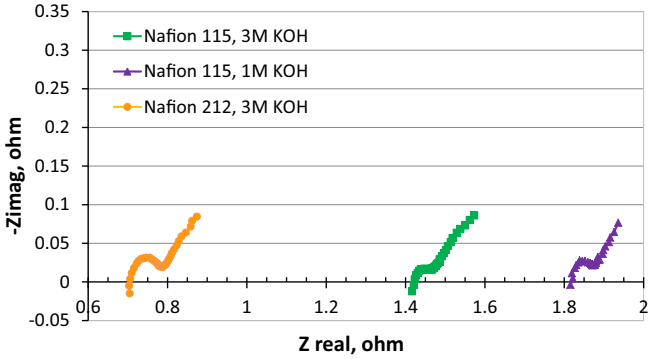

Figure 4. Study 2: Internal impedance of the alkaline H_2-Br_2 fuel cell with Nafion 115 & 212 membranes and different KOH concentrations.

The results in Figures 3a and 3b show that significant performance improvement was obtained in the second study when new electrode designs, interdigitated flow fields, thinner membranes and higher KOH concentrations were used. Both thinner membranes and higher KOH concentrations led to lower slopes in the discharge and charge polarization curves and consequently higher fuel cell performance. The slopes of these curves represent all the resistances in the fuel cell such as electronic, ohmic, kinetics and transport resistances; so changes in the slope can be attributed to changes in the KOH concentration and membrane. Losses due to the electrical components such as the hydrogen and bromine electrodes, flow field plates, current collectors and electrical contact resistance are typically small, around 100 milliohms (or 44.4 milliohm cm^{-2}); while losses due to the ionic components such as the cation conducting membrane and electrolytes (KOH and KBr/Br_2) in the hydrogen and bromine half-cells are much higher. Note that high KOH concentration provides high ionic conductivity and high OH^- concentration, which is especially important during discharge. During discharge, the consumption of OH^- ions and generation of water by the hydrogen oxidation reaction can lead to a rapid decrease in the KOH concentration. This explains the smaller voltage losses obtained for charge than compared to discharge. During charge, water is consumed and KOH is generated making the electrolyte in the hydrogen electrode more conductive. For the alkaline-based H_2-Br_2 and H_2-I_2 reversible fuel cells, it is worth noting here that when KOH is produced at the negative electrode (increasing the ionic conductivity) during charge, KBr/KI is consumed at the positive electrode (decreasing the ionic conductivity). The opposite phenomenon occurs during discharge (ionic conductivity decreasing at the negative electrode and increasing at the positive electrode). Due to the combined effect of KOH production and H_2O consumption at the negative electrode, we expect the change in ionic conductivity at the negative electrode to have a larger impact on fuel cell performance than the change in the positive electrode's ionic conductivity. The best performance was obtained with 3 M KOH solution and the 51-micron Nafion 212 membrane. The fuel cells with 3 M KOH also benefit from a high open circuit voltage resulting from a more negative hydrogen electrode potential. Note also that the discharge and charge curves remain linear while the cell current densities were much higher in this study. For the second study, the fuel cell performance is still dominated by the ohmic resistance in the cell. The previously observed mass transport effect in the hydrogen electrode at low current density in the first study has been resolved by the improved hydrogen electrode design.

In the second study, the fuel cell internal resistances were measured at the three conditions using EIS in order to determine the contribution of the ohmic resistance of the cell to the electrochemical performance. The overall cell internal resistance was measured by using the hydrogen electrode as the reference electrode. As shown in Figure 4, the intersection of the left-hand edge of each curve with the horizontal zero imaginary impedance occurs at high frequency and represents the pure ohmic resistance of the fuel cell. The intersection of the right-hand edge of each curve, before the 45-degree angle

Downloaded on 2017-07-31 to IP 147.8.230.58 address. Redistribution subject to ECS terms of use (see ecsdl.org/site/terms_use) unless CC License in place (see abstract).

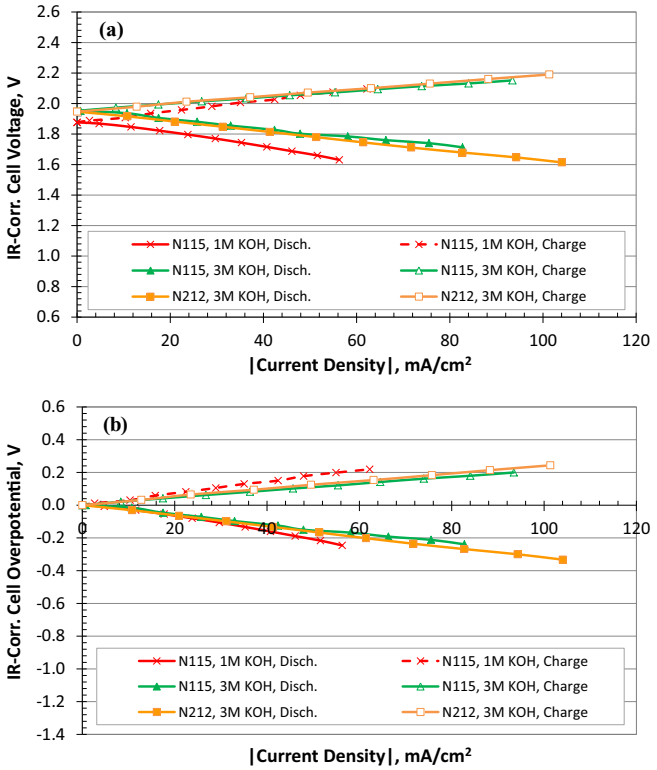

Figure 5. Study 2: IR corrected discharge and charge polarization curves of the alkaline H_2-Br_2 fuel cell, cell overpotential was used in (b) to correct for different OCVs.

tail, occurs at lower frequency and represents the combined ohmic and charge transfer resistance in the fuel cell. The ohmic resistance (left-hand edge of the semicircle) was highest (~1.82 ohms) for the case with the thicker membrane (Nafion 115) and lower KOH concentration (1 M). The lowest internal resistance (0.7 ohms) and best performance was obtained using the thinner membrane (Nafion 212) and higher KOH concentration (3 M). The conductivity of the K^+-form membrane was measured, using a conductivity cell, to be about 0.006 S/cm (versus 0.070 S/cm for the same membrane in H^+-form). Based on the thickness (~51 microns for Nafion 212) and active area (2.25 cm^2) of the membrane, the resistance attributable to the membrane is about 0.4 ohm (best case). The high membrane resistance and the additional resistance of the KOH compartment result in the high internal resistance for these cells, which is about 7 to 10 times higher than of an acid-based H_2-Br_2 fuel cell. To obtain better performance, the internal resistance of the alkaline system needs to be reduced further. Finally, the low charge transfer resistance, the difference between the combined resistance and the pure ohmic resistance, confirms that the kinetics of the hydrogen and bromine electrode reactions in this alkaline H_2-Br_2 fuel cell are quite fast.

In the second study, the internal resistances were used to remove the effect of the IR losses in the cell due to the different KOH concentrations and membrane thicknesses in order to evaluate the kinetic and transport effects. The IR-corrected cell voltages and overpotentials for these three runs are shown in Figures 5a and 5b. The results in Figure 5b show that after the ohmic losses and the difference in the OCV due to KOH concentration are removed, the performance of the 1 M and 3 M KOH concentration cases are quite similar. They showed similar voltage losses due to kinetics and concentration polarization at the two electrodes. At the lower 1 M KOH concentration, there appears to be a more significant transport effect during discharge and charge at current densities above 20 mA/cm^2. Finally, the power density for these runs are provided in Figure 6.

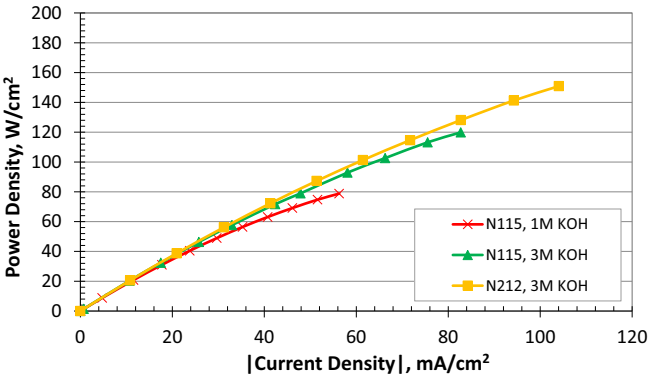

Figure 6. Study 2: Discharge power density of the alkaline H_2-Br_2 fuel cell tested with different KOH concentrations and membrane thicknesses.

Studies 3 and 4.—Studies 3 and 4 were completed to evaluate the performance of the alkaline H_2-I_2 fuel cell. As described earlier, two different cell configurations were used. The configuration shown in Figure 1c (for study 3) was used first to validate the concept and to evaluate the cell and individual electrode performances, as well as the effect of KOH concentration. The configuration shown in Figure 1d (for study 4) was used to evaluate the concept of two-phase (gaseous hydrogen and liquid KOH) reactant feed to the negative electrode.

For study 3, the full-cell and half-cell voltages at OCV are shown in Figure 7a. These results confirm the higher anticipated cell voltage and the more negative hydrogen reaction potential in an alkaline (i.e., high pH) medium. Figure 7b shows the discharge and charge polarization curves for the same fuel cell at three different KOH concentrations (1 M–3 M). As observed in the H_2-Br_2 study, the OCV shifted higher and the discharge performance improved with increasing KOH concentration. The charge performance did not vary much with increasing KOH concentration because during charge the hydrogen electrode reaction generates KOH and consumes H_2O, leading to higher conductivity and lower ohmic resistance in the electrode.

For study 3, we were able to measure the internal resistance of the full cell and two half-cells by inserting a platinum wire into the

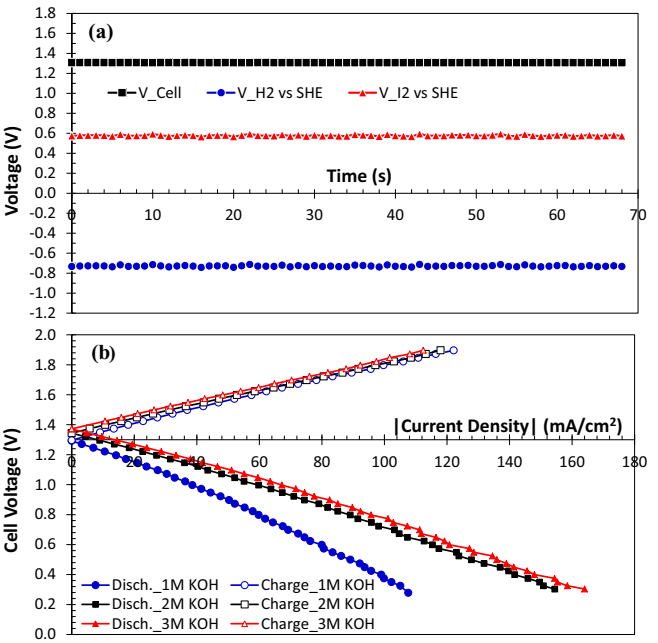

Figure 7. Study 3: Cell and individual electrode potentials of the alkaline H_2-I_2 fuel cell during (a) open circuit and (b) charge and discharge.

Downloaded on 2017-07-31 to IP 147.8.230.58 address. Redistribution subject to ECS terms of use (see ecsdl.org/site/terms_use) unless CC License in place (see abstract).

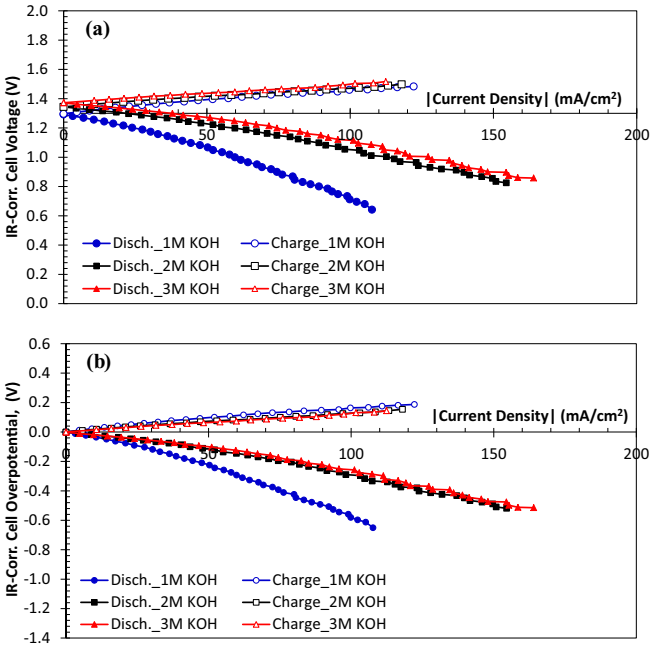

Figure 8. Study 3: IR corrected cell voltage (a) and cell overpotential (b) of the alkaline H_2-I_2 fuel cell showing better performance with increasing KOH concentration.

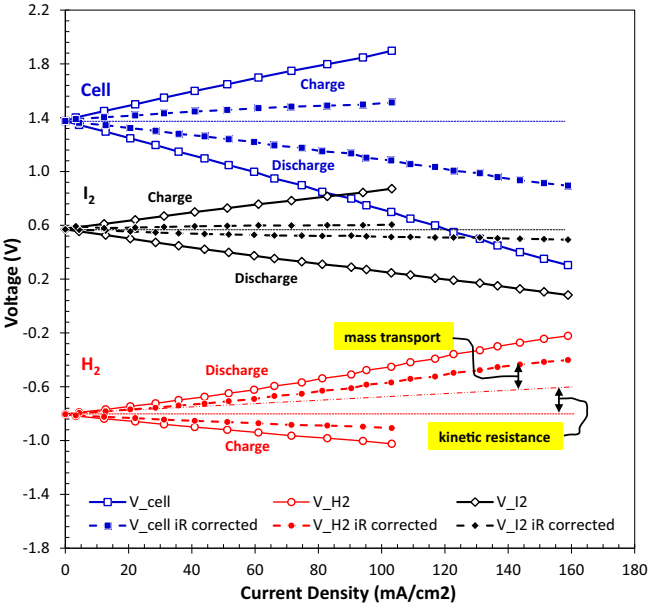

Figure 9. Study 3: Polarization curves of the full cell, H_2 half-cell, and I_2 half-cell of the alkaline H_2-I_2 fuel cell with 3 M KOH concentration before and after IR correction. Results show the fuel cell performance is dominated by the H_2 electrode.

KOH compartment. For the 1 M KOH case, the resistances were measured to be 2.2 ohms for the full cell, 0.65 ohms for the hydrogen half-cell, and 1.55 ohms for the iodine half-cell. The cell internal resistance is quite high, higher than that of the alkaline H_2-Br_2 cells, and could be attributed to the higher contact resistance between the current collectors, flow field plates and gas diffusion electrodes due to using a low cell compression (<788 kPa versus 1475 kPa). A low cell compression was used in order to avoid crushing the glass fiber mat in the KOH compartment. Note that with the location of the platinum sensing wire, the internal resistance of the iodine half-cell includes the resistance of the K^+-form Nafion membrane and most of the KOH solution in the negative electrolyte compartment. Based on the conductivity, thickness (~51 microns), and active area (2.25 cm^2) of the K^+-form Nafion 212 membrane, the resistance attributable to the membrane is about 0.4 ohm. Based on the thickness of the KOH compartment (1 mm) and the conductivity of 1 M KOH (~0.2 S/cm), the contribution of the KOH compartment to the cell resistance is about 0.2 ohms or more. The high remaining resistances of the two half-cells were attributed, as mentioned earlier, to the high contact resistance between the components in the cell. This problem could be minimized by eliminating the KOH compartment in order to allow higher cell compression.

In order to remove the effect of ohmic losses in the cell so that the effect of kinetics and mass transport on cell performance could be evaluated, the cell voltages were corrected for IR-loss using the cell impedance measured at open circuit. The resulting polarization curves are shown in Figures 8a and 8b. Figure 8a shows the IR-corrected cell voltage versus the absolute of the current density while Figure 8b shows the cell overpotential (difference between the cell IR-corrected voltage and cell OCV). Plotting the cell overpotential allows us to remove the effect of the KOH concentration on the OCV. From these results it is quite clear that the discharge performance of the H_2-I_2 fuel cell with 1 M KOH at the flow rate used in the study shows significant mass transport effect, starting at current density as low as 20 mA/cm^2. This mass transport effect at low current density can be attributed to the rapid decrease in the OH^- concentration during discharge as a result of both OH^- consumption and the dilution effect from H_2O generation on the hydrogen reaction. As shown in Figure 8b, the mass transport effect of OH^- depletion on the fuel cell discharge performance is reduced, but not eliminated, when higher KOH concentrations are used. It is worth pointing out here that since IR correction was done using the cell internal resistance at open circuit, some IR loss component still exists in the polarization curves at high current densities when the concentrations of active species continue to change. On the other hand, close observation of the charge curves reveals that the slope of the polarization curves decreases slightly as the current density increases. This is attributed to the production of OH^- and consumption of H_2O leading to higher KOH electrolyte conductivity in the hydrogen electrode and hence lower IR losses in the cell.

With the reference electrode and platinum sensing wires in the KOH compartment, the fuel cell performance can be separated into half-cell performances. The results can be used to identify the limiting electrode and limiting process at each electrode. Figure 9 shows the fuel cell discharge and charge polarization curves before and after IR correction for the 3 M KOH case. The discharge and charge curves for the hydrogen and iodine half-cells before and after IR correction are also provided in Figure 9. For IR correction, the half-cell resistances are measured using the Pt sensing wire in the KOH compartment as the reference electrode, whereas the full cell resistance is measured using the hydrogen electrode as the reference electrode. These results show that the iodine electrode performed much better than the hydrogen electrode. The iodine electrode exhibits very little activation and transport losses. The hydrogen electrode, whose reactions are known to be 2–3 orders of magnitude slower in alkaline media than acidic media,[23] shows much higher activation loss during both charge and discharge, as well as significant transport polarization during discharge. A double dotted line extrapolated from the linear region of the discharge curve at low current density, representing the hydrogen polarization curve without transport resistance, is inserted to show the voltage loss that can be attributed to transport loss at the negative hydrogen electrode. This transport loss is associated with the difficulty of creating a three-phase (gas-liquid-solid) reactive surface and transporting gaseous hydrogen reactant simultaneously with liquid KOH to this surface. Finally, the power density curves for the three runs of study 3 are provided in Figure 10. The power densities of this alkaline fuel cell system are not as high as those of the H_2-Br_2 system because of its lower fuel cell voltage.

Downloaded on 2017-07-31 to IP 147.8.230.58 address. Redistribution subject to ECS terms of use (see ecsdl.org/site/terms_use) unless CC License in place (see abstract).

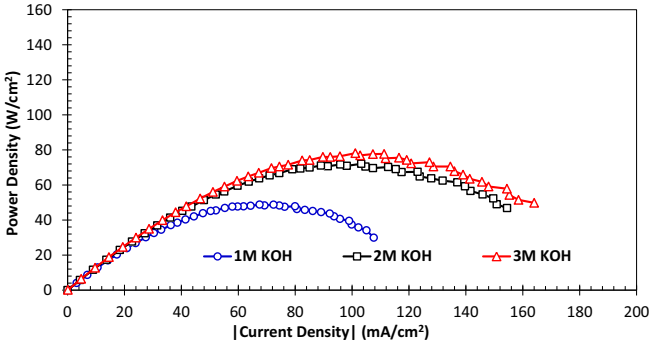

Figure 10. Study 3: Discharge power density of the alkaline H_2-I_2 fuel cell tested with different KOH concentrations.

Finally, the alkaline H_2-I_2 fuel cell system with two-phase reactant feed (study 4) at the negative electrode was evaluated. A 3 M KOH solution was used for this study. By using two-phase feed, the KOH compartment was eliminated. This resulted in a reduction in the cell internal resistance from 2.2 ohms to 1.3 ohms, lower ohmic slope in the polarization curve during discharge and charge, and better performance as shown in Figures 11a and 11b. The cell open circuit voltage was slightly shifted because of the higher hydrogen gas pressure needed to force liquid KOH out of the electrode. Peak power increased by 36% with this new two-phase feed configuration. The IR-corrected results in Figure 11b, with visual compensation for the vertical shift in the OCV, show reduced mass transport effect during discharge with this new feed approach. To confirm that the improved mass transport effect was at the negative hydrogen electrode, the cell IR-corrected voltage was decomposed into half-cell IR-corrected overpotentials using the reference electrode. The reference electrode was ionically connected to the positive electrode through a KI electrolyte bridge. Note that due to the location of the reference electrode, the IR voltage

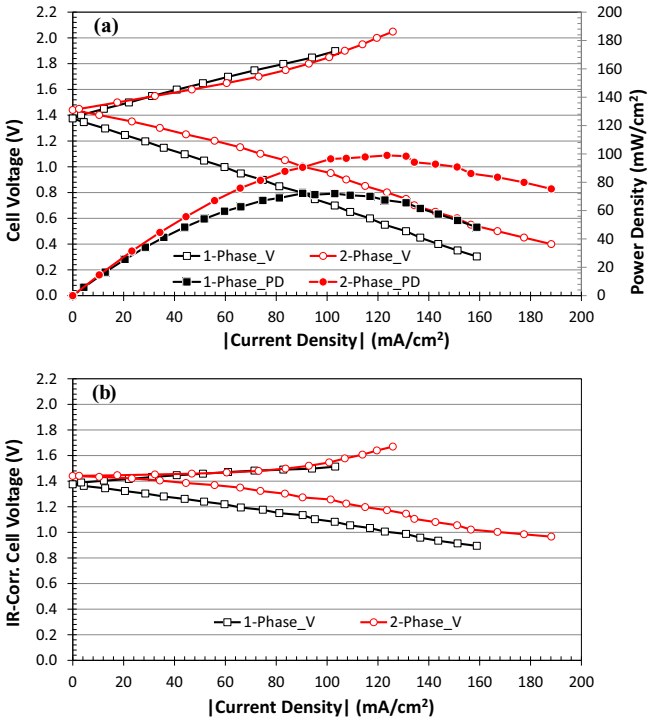

Figure 11. Study 4: Polarization and discharge power density curves of the alkaline H_2-I_2 fuel cell tested at 3 M KOH with two-phase negative electrode in configuration 3d in comparison to single-phase electrode in configuration 3c, before (a) and after (b) IR correction.

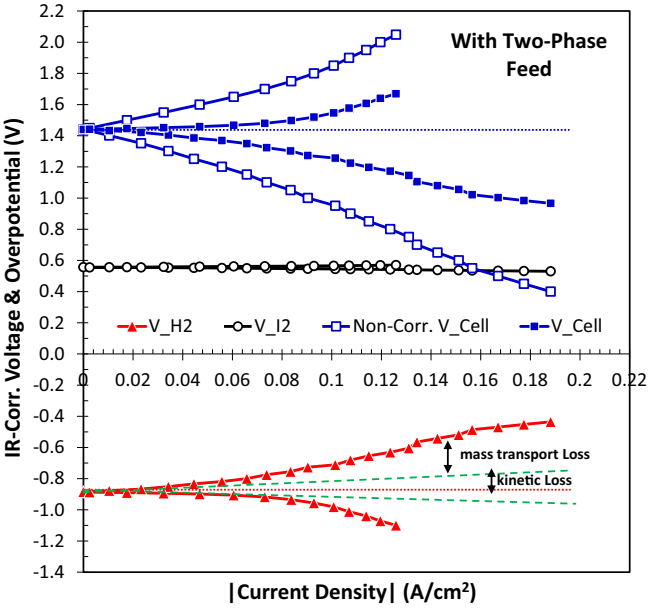

Figure 12. Study 4: IR-corrected polarization curves of the full cell, H_2 half-cell, and I_2 half-cell of the alkaline H_2-I_2 fuel cell with 3 M KOH concentration and two-phase negative electrode feed. Results show the performance of this H_2-I_2 fuel cell is still dominated by the H_2 electrode.

loss in the cell was applied to the hydrogen half-cell. From the results in Figure 12, it is clear that the overpotential at the iodine electrode was quite small and most of the kinetic and mass transport losses in the fuel cell were attributed to the hydrogen electrode. As before, two dash lines extrapolated from the linear region at low current density were inserted to help separate the voltage loss due to mass transport from that of kinetics. During discharge, mass transport effect started at low current density (~30 mA/cm^2) and is attributed to the rapid decrease in OH^- concentration. During charge, the mass transport effect started at a higher current density (~ 90 mA/cm^2) and is attributed to the increase in the hydrogen gas evolution rate. The increase in hydrogen gas production decreases the transport rate of aqueous KOH to the negative electrode's surface. Since water is consumed at the negative electrode during charge, the shortage of aqueous KOH solution leads to a sharp increase in the overpotential.

Summary

The alkaline H_2-Br_2 and H_2-I_2 fuel cells are attractive because of their advantages over the acidic systems such as higher cell voltage and lower cost catalysts for the hydrogen evolution and oxidation reactions. Fuel cells were assembled to validate the feasibility of these alkaline systems and to evaluate their performance under various configurations and conditions. Some of the conditions evaluated were high KOH concentration and thinner cation exchange membranes. For the alkaline H_2-I_2 fuel cell, two configurations were used to evaluate the effectiveness of single-phase versus two-phase reactant feed for the hydrogen reaction at the negative electrode.

The results confirmed that the alkaline H_2-Br_2 and H_2-I_2 fuel cells have a higher cell voltage than the acidic system, while maintaining fast electrode reaction kinetics. However, the performance of these alkaline systems is currently limited by high internal resistance of the existing electrode and cell design. A significant fraction of the internal resistance is caused by the low ionic conductivity of the K+ conducting membranes. The discharge and charge performances of these systems are controlled by the performance of the hydrogen negative electrode. A porous electrode that has more optimal three-phase distribution and can handle two-phase feed is expected to have a major impact on fuel cell performance. Future

Downloaded on 2017-07-31 to IP 147.8.230.58 address. Redistribution subject to ECS terms of use (see ecsdl.org/site/terms_use) unless CC License in place (see abstract).

studies should include long-term durability testing of these alkaline fuel cell systems. During long-term operation, hydroxide crossover could cause an increase in the positive electrolyte pH over time and may impact long-term performance. Other areas for future studies should include non-precious alloy catalysts with high hydrogen oxidation and evolution (HER/HOR) activity, more conductive and perm-selective membranes, and evaluation of the effect of chemical products that could form from the crossover of OH^-, Br^- and Br_2.

Acknowledgments

This work was funded in part by the National Science Foundation through grant number EFRI-1038234 and the Research Grants Council of Hong Kong through a General Research Fund (GRF HKU 700210P).

References

1. Livshits A. Ulus and E. Peled, "High-power H_2/Br_2 fuel cell," *Electrochem. Comm.*, **8**, 1358 (2006).
2. Haley Kreutzer, Venkata Yarlagadda, and Trung Van Nguyen, "Performance Evaluation of a Regenerative Hydrogen Bromine Fuel Cell," *J. Electrochem. Society*, **159**, F331 (2012).
3. Kyu Taek Cho, Paul Ridgway, Adam Z. Weber, Sophia Haussener, Vincent Battaglia, and Venkat Srinivasan, *J. Electrochem. Soc.*, **159**, A1806 (2012).
4. Kyu Taek Cho, Paul Albertus, Vincent Battaglia, Aleksandar Kojic, Venkat Srinivasan, and Adam Z. Weber, *Energy Technology*, **1**, 557 (2013).
5. A. Ivanovskaya, N. Singh, R.-F Liu, H. Kreutzer, J. Baltrusaitis, T. V. Nguyen, H. Metiu, and E. W. McFarland, "Transition Metal Sulfide Hydrogen Evolution Catalysts for Hydrobromic Acid Electrolysis," *Langmuir*, **29** (1), 480 (2013).
6. Venkata Yarlagadda, Regis P. Dowd Jr., Jun Woo Park, Peter Pintauro, and Trung Van Nguyen, "A Comprehensive Study of an Acid-Based Reversible H_2-Br_2 Fuel Cell System," *J. Electrochem. Soc.*, **162** (8), F919 (2015).
7. Jahangir Masud, Trung Van Nguyen, Nirala Singh, Eric McFarland, Myles Ikenberry, Keith Hohn, Chun-Jern Pan, and Bing-Joe Hwang, "A RhxSy/C Catalyst for the Hydrogen Oxidation and Hydrogen Evolution Reactions in HBr," *J. Electrochem. Soc.*, **162** (4), F455 (2015).
8. Michael C. Tucker, Kyu Taek Cho, Adam Z. Weber, Guangyu Lin, and Trung Van Nguyen, "Optimization of Electrode Characteristics for the Br_2/H_2 Redox Flow Cell," *J. Appl. Electrochem.*, **45**, 11 (2015).
9. Guangyu Lin, Pau Ying Chong, Venkata Yarlagadda, Trung Nguyen, Ryszard Wycisk, Peter Pintauro, Michael Bates, Sanjeev Mukerjee, Michael Tucker, and Adam Weber, "Advanced Hydrogen-Bromine Flow Batteries," *J. Electrochemical Society*, **163** (1) A5049 (2016).
10. Venkata Yarlagadda and Trung Van Nguyen, "High Active Surface Area and Durable Multi-Wall Carbon Nanotube-Based Electrodes for Bromine Reactions in H_2-Br_2 Fuel Cells," *J. Electrochemical Society*, **163** (1) A5134 (2016).
11. Venkata Yarlagadda and Trung Van Nguyen, "High Surface Area Carbon Electrodes for Bromine Reactions in H_2-Br_2 Reversible Fuel Cells," *J. Electrochemical Society*, **163** (1) A5126 (2016).
12. Jun Woo Park, Ryszard Wycisk, Peter Pintauro, Venkata Yarlagadda, and Trung Van Nguyen, "Electrospun Nafion/Polyphenylsulfone Composite Membranes for Regenerative Hydrogen Bromine Fuel Cells," *Materials*, **9**(3), 143 (2016).
13. Trung Van Nguyen, Venkata Yarlagadda, Guangyu Lin, Guoming Weng, Chi-Ying Vanessa Li, and Kwong-Yu Chan, "Comparison of Acid and Alkaline Hydrogen-Bromine Fuel Cell Systems," *ECS Transactions*, **58**(37), 29 (2014).
14. W. Sheng, A. P. Bivens, M. Myint, Z. Zhuang, R. V. Forest, Q. Fang, J. G. Chen, Y. Yan, and "Non-precious Metal Electrocatalyst with High Activity for Hydrogen Oxidation Reaction in Alkaline Electrolytes", *Energy & Environmental Science*, **7**, 1719 (2014).
15. Shanfu Lu, Jing Pan, Aibin Huang, Lin Zhuang, and Juntao Lu, "Alkaline polymer electrolyte fuel cells completely free from noble metal catalysts," *PNAS*, **105** (52), 20611 (2008).
16. Anneke Hauch and Andreas Georg, "Diffusion in the electrolyte and charge-transfer reaction at the platinum electrode in dye-sensitized solar cells," *Electrochimica Acta*, **46**, 3457 (2001).
17. Gerrit Boschloo and Anders Hagfeldt, "Characteristics of the Iodide/Triiodide Redox Mediator in Dye-Sensitized Solar Cells," *Accounts of Chemical Research*, **42**, 1819 (2009).
18. Qing Zhao, Yanying Lu, Zhiqiang Zhu, Zhangliang Tao, and Jun Chen, "Rechargeable Lithium-Iodine Batteries with Iodine/Nanoporous Carbon Cathode," *Nano Letters*, **15**, 5982 (2015).
19. Yu Zhao, Lina Wang, and Hye Ryung Byon, "High-Performance Rechargeable Lithium-Iodine Batteries Using Triiodide/Iodide Redox Couples in an Aqueous Cathode," *Nature Communications*, **4**, 1896 (2013).
20. B. Li, Z. Nie, V. Murugesan, E. Thomsen, D. Reed, J. Liu, W. Wang, and V. Sprenkle, "Optimization of High-Energy-Density Aqueous Zinc-Polyiodide Redox Flow Battery," *Electrochemical Society Spring 2015 Meeting*, Abstract No. 684, Chicago, Illinois, 2015.
21. Trung V. Nguyen, "A Gas Distributor Design for Proton Exchange Membrane Fuel Cells," *J. Electrochem. Society*, **143**, L103 (1996).
22. Trung Van Nguyen and Wensheng He, "Interdigitated Flow Field Design," *Handbook of Fuel Cells: Fundamentals, Technology and Applications*, Volume III, Part 3, pp. 325, Eds. W. Vielstich, A. Lamm, and H. Gasteiger, Wiley, New York, NY, 2003.
23. W. Sheng, H. A. Gasteiger, and Y Shao-Horn, *J. Electrochem. Soc.*, **157**, B1529 (2010).

Downloaded on 2017-07-31 to IP 147.8.230.58 address. Redistribution subject to ECS terms of use (see ecsdl.org/site/terms_use) unless CC License in place (see abstract).